J. Indian Inst. Sci., Jul–Aug. 2001, **81**, 491–510

IISc THESIS ABSTRACTS

Thesis Abstract (Ph. D.)

Studies on hydrolytic and thermal degradations of polyphosphate esters by N. Narendran
Research supervisor: Prof. D. N. Sathyanarayana
Department: Inorganic and Physical Chemistry

1. Introduction

When there are hydrolysable linkages present in a polymer, as in condensation polymers such as polyesters, polyanhydrides, etc., the polymer can be degraded by water. This is known as hydrolytic degradation. When hydrolytic degradation is catalysed by enzymes, it is referred to as biodegradation. Thus, hydrolytically degradable polymers are of interest because of their application in biomedical field. Of the polymers studied so for, very little work has been reported on polyphosphate esters. Hence, a detailed investigation of the hydrolytic degradation of polyphosphate esters was undertaken. Polyphosphate esters are also well known for their flame retardancy.

2. Experimental

A typical procedure for the synthesis of polyphosphate ester homopolymers is as follows: The bisphenol (0.07 m), sodium hydroxide (0.02 m) and the phase-transfer catalyst tetrabuty1 ammonium bromide (10 mo1%, 0.007 m) were taken in a 3-necked round bottom flask attached with a nitrogen inlet, addition funnel and a mechanical stirrer. The mixture in the flask was dissolved in 120 ml of water. Afterwards, while stirring the mixture vigorously, freshly distilled phenyl phosphorodichloridate (0.067 m, 10 ml) dissolved in 100 ml of dry dichloromethane solvent, was added rapidly to the mixture using an addition funnel. The reaction mixture was further stirred vigorously for 30 minutes.

The organic layer was separated from the aqueous layer, washed with water and reprecipitated in petroleum ether. The solid polymer was washed with water to remove traces of phase-transfer catalyst. The copolymers and the terpolymer were synthesized in a similar manner except that the feed ratio of the bisphenols is 50:50% for the copolymers and 33.33% each for the terpolymer.

The polymers were characterized by infrared, ^{1}H, ^{13}C and ^{31}p NMR sepectroscopy. Hydrolytic degradation studies were carried out by making polymer pellets and exposing them to NaOH solution. The degradation was monitored by the weight loss of the pellets. The studies on diffusion of NaOH solution into the polymer were accomplished in thick-walled glass capillary tubes containing the polymer powder. Thermal degradation of the polymers was performed by thermogravimetry and pyrolysis GC-MS.

3. Results and discussion

Five homopolymers (I–V) were synthesized by interfacial polycondensation of phenylphosphorodichloridate with bisphenol-A, bisphenol-S, phenolphthalein, biphenol and thiodiphenol, respectively (Scheme 1). Two copolymers were synthezized by polycondensation of

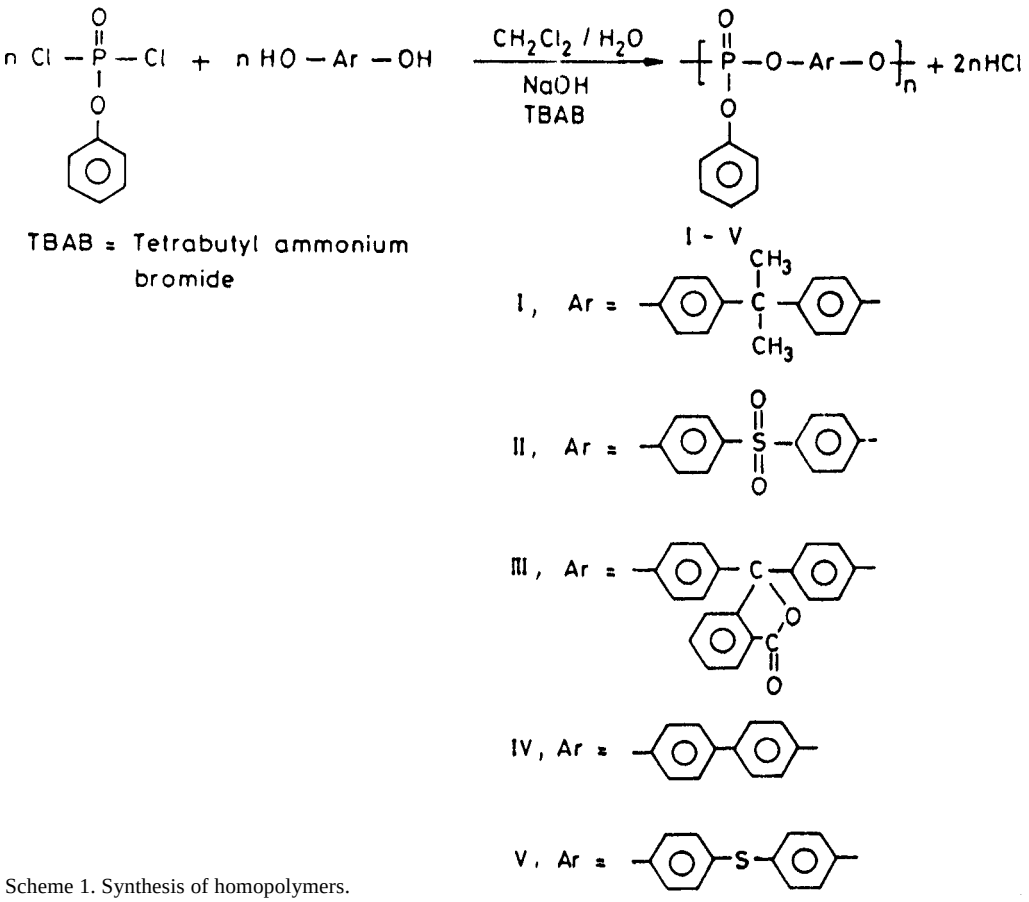

Scheme 1. Synthesis of homopolymers.

phenylphosphorodichloridate with a mixture of bisphenol-A with biphenol (VI), a mixture of bisphenol-A with thiodiphenol (VII) and a terpolymer (VIII) when the three bisphenols, namely, bisphenol-A, biphenol and thiodiphenol are present.

All the polymers are white powdery solids except the polymer from biphenol. The yields of the polymers vary from a low value of 54% for polymer III to a high value of 82% for polymer VI and VIII.

All the polymers were characterized by FT-IR, ^{1}H, ^{13}C and ^{31}p NMR spectroscopic techniques. The composition ratio of the copolymers and the terpolymer was determined by ^{1}H NMR spectroscopy. The molecular weights of the polymers were also determined by ^{31}p NMR spectroscopy.

To begin with a detailed investigation on the polymer synthesized from bisphenol-A was undertaken. The accelerated hydrolytic degradation, under alkaline conditions, was performed at various concentrations of NaOH and at different temperatures. A typical plot of the degradation is shown in Fig. 1. The rate of degradation increases with increase in concentration of NaOH,

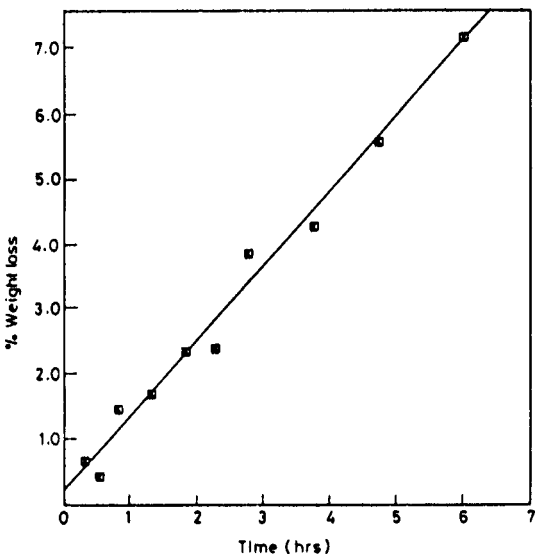

Fig. 1. Plot of weight loss vs time in 6 M NaOH.

reaches a maximum at 6M NaOH and then decreases. It was found that the diffusion of alkali also plays an important role and therefore diffusion studies of NaOH solution into the polymer powder inside a thick-walled glass capillary tube were carried out. Here too the maximum rate of diffusion was found to occur at 6M NaOH solution. The activation energy for the diffusion process was found to be 12 kcal/mol. A comparative study of the hydrolytic degradation of the other polymers showed that the polymer synthesized from biphenol is the most stable and the one obtained from thiodiphenol is the least stable one.

Thermal degradation studies were also carried out on the polymers by thermogravimetry and pyrolysis GC-MS. About 20 to 44 degradation products were detected in the pyrolysis of these polymers at 740^{O}C. Phenol is the major product in all the polymers. Mechanisms for the formation of the major products of degradation have been proposed.

References

1. SUDESH, K. G. — *Biodegradable polymers: Prospects and progress*, Marcel Dekker, 1986.
2. LI, N. H., RICHARDS, M., BRANDT AND LEONG, K. W. — *Polymer preprints, Am. Chem. Soc. Div. Polym. Chem.* 1989, **30** (1), 454.
3. LUO, Y., ZHUO, R. AND FAN, C. L. — *Chin. Chem. Lett.*, 1995, **6**, 333.
4. RICHARDS, M., DAHIYAT, B. I., ARM, D. M. LINS, S. AND LEONG, K. W. — *J. Polym. Sci. Polym. Chem.*, 1991, **29**, 1157.
5. BARNARD, D. W. C., BUNTON, C. A. LLEWELLYN, D. R., VERNON, C. A. AND WELCH, V. A. — *J. Chem. Soc.*, 1961, 2670.

Thesis Abstract (Ph. D.)

Late transition metal complexes of chiral and unsymmetrical diphosphazanes by K. Raghuraman
Research supervisor: Prof. S. S. Krishnamurthy
Department: Inorganic and Physical Chemistry

1. Introduction

In recent years there has been an increasing awareness of the importance of ligands based on P-N-P framework in transition metal organometallic chemistry because of possible applications of such complexes in homogeneous catalysis.[1–4] The following topics have been investigated in the present study:

1. Reactions of diphosphazanes with various ruthenium derivatives,
2. Syntheses and transition metal chemistry of diphosphazane monosulfides,
3. Reactions of diphosphazanes with various rhenium derivatives,
4. Synthesis of an unsymmetrical chiral diphosphazane and its palladium complex, and
5. A preliminary investigation on asymmetric hydrogenation using rhodium complexes of chiral diphosphazanes and diphosphazane monosulfides.

2. Results and discussion

Reactions of diphosphazanes $Ph_2PN(R)PPh_2$ (R=(*S*)-*CHMePh **L**[1], $CHMe_2$ **L**[2]) with $[RuCl_2(PPh_3)_3]$ or $[RuCI_2(cod)]_n$ (cod = 1,5-cyclooctadiene) give *trans*-[RuXCI]{η^2-(**L**[1] or **L**[2])}$_2$] (X = CL or H). Reactions of $[CpRu(PPh_3)_2CI]$ (**A**) (Cp = η^5-C_5H_5) with achiral diphosphazanes, $X_2PN(CHMe_2)PYY'$ (X = Y = Y' = Ph; X = Ph, YY' = $O_2C_6H_4$; X_2 = YY' = $O_2C_6H_4$) yield cationic mononuclear complexes chelated and/or η_1-coordinated diphosphazanes depending on the diphosphazanes used. Reactions of **A** with chiral racemic diphosphazanes $Ph_2PN(CHMe_2)PYY'$ (YY' = $O_2C_{20}H_{12}$; Y = Ph, Y' = OC_6H_4Me-4, $OC_6H_3Me_2$-3,5 or $N_2C_3HMe_2$-3,5) afford both diastereomeric ruthenium complexes (*dl* and *meso*); the formation of only one diastereomeric complex is observed in some cases. Reaction of **A** with chiral symmetrical diphosphazane **L**[1] gives both the neutral [CpRu{η^2-(**L**[1])}C1] (**1**) and the cationic complex [CpRu{η^2-(**L**[1])}PPh_3]C1 (**2**). Treatment of the chiral unsymmetrical diphosphazane (*SR*)-Ph_2PN(*CHMePh)P* (Ph)($N_2C_3MHe_2$-3,5) (**L**[3]) with **A** yields a novel neutral trichiral ruthenium complex ($S_CS_PR_{Ru}$)-[CpRu*{η^2-(**L**[3])}C1] (**3**) and the cationic complex ($S_CS_PR_{Ru}$) or ($S_CS_PS_{Ru}$)-[CpRu*{η^2-(**L**[3])}PPh_3]C1. The reaction of a diastereomeric mixture of the diphosphazane (*SR*),(*SS*)-Ph_2PN(*CHMePh)P*Ph($N_2C_3HMe_2$-3,5) with **A** affords diastereomeric neutral cationic complexes. The labile Ru-CI bond in **1** is

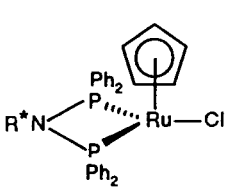

1

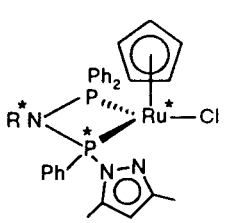

$S_CS_PR_{Ru}$ **3**

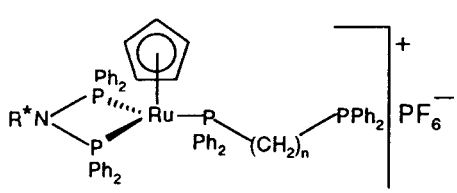

n = 1 (**4**),
n = 2 (**5**)

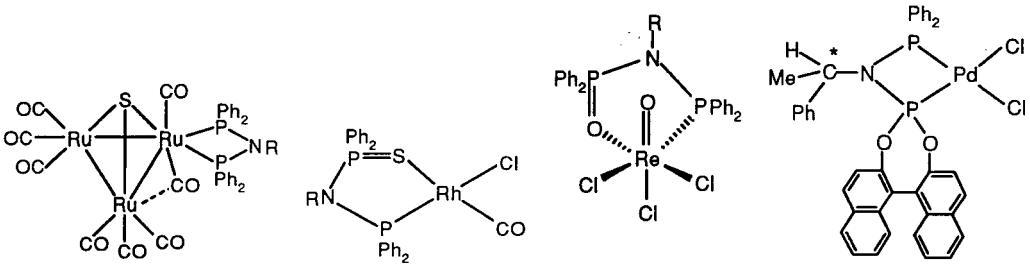

readily replaced by PX_3 (X = Ph or OMe) or $Ph_2P(CH_2)_nPPh_2$ (n = 1 or 2), e.g. **4** and **5**. Reactions of **1** with various organic reagents have also been investigated.

Treatment of the diphosphazane monosulfides $Ph_2PN(R)P(S)Ph_2$ (R = (*S*)=*CHMePh (**L^{1}S**), $CHMe_2$ (**L^{2}S**)) with Ru3*CO)$_{12}$ gives the trinuclear sulfur monocapped ruthenium clusters, [Ru_3-(μ_3-S)(μ-CO)(CO)$_7${η^2-($Ph_2PN(R)PPh_2$)}]. The reactions of **L^{1}S** or **L^{2}S** with [RhC1(CO)$_2$]$_2$ and [Rh(cod)$_2$]BF_4 give *cis*-[Rh(CO)C1{η^2-(**L^{1}S** or **L^{2}S**)}] and [Rh{η^2-(**L^{1}S** or **L^{2}S**)}$_2$]BF_4, respectively. The reactions of **L^{1}S** or **L^{2}S** with [MC1$_2$(cod)] (M = Pd, pt) yield monomeric *cis*-chelated complexes [MC1$_2${η^2-(**L^{1}S** or **L^{2}S**)}$_2$].

The reaction of diphosphazane **L^2** with Re_2O_7 gives the unusual Re^V/Re^{VII} complex [ReO_2{η^2-(**L^2**)}$_2$]ReO_4. Reactions of **L^1** and **L^2** with [ReOC1$_3$(PPh_3)$_2$] give the diphosphazane monoxide coordinated complexes [ReOC1$_3${η^2-($Ph_2PN(R)P(O)Ph_2$)}](**8**).

The unsymmetrically substituted chiral diphosphazane (*SR*), (*SS*)-($H_{12}C_{20}O_2$)PN (*CHMe-Ph)PPh_2 (**L^4**) bearing the C2-symmetric binapthylene dioxy unit has been synthesized. Reaction of this diastereomeric mixture with [PdC1$_2$(cod)] affords (*SR*) and (*SS*) diastereomeric palladium complexes, *cis*-[PdC1$_2${η^2-(**L^4**)}] of which the (*SR*) diastereomer (**9**) has been separated by fractional crystallization.

A preliminary investigation on asymmetric hydrogenation of itaconic acid (CH_2=C(COOH)CH_2COOH) to methylsuccinic acid using rhodium complexes of diphosphazanes and diphosphazane monosulfide indicate that diphosphazanes bearing C_2-chiral binapthylene dioxy moiety increases the enantiomeric excess.

3. Experimental

All the reactions were carried out using standard Schlenk techniques and solvents were purified prior to use. The diphosphazane ligands Ph_2PN(*CHMePh)PPh_2,[5] $Ph_2PN(CHMe_2)PPh_2$,[6] $Ph_2PN(CHMe_2)P(O_2C_6H_4)$,[7] ($H_4C_6O_2$)$PN(CHMe_2)P(O_2C_6H_4)$,[8] (*SR*),(*SS*)-$Ph_2PN$(*CHMePh)*PPh($N_2C_3HMe_2$-3,5),[5] $Ph_2PN(CHMe_2)PPh(N_2C_3HMe_2$-3,5),[7] and $Ph_2PN(CHMe_2)PPh(OR)$ (R = C_6H_4Me-4, $C_6H_3Me_2$-3,5)[7] were synthesized as reported in the literature.

The complexes *trans*-[RuC1$_2${η^2-(**L^1** or **L^2**)}$_2$] were prepared by the reactions of [RuC1$_2$(PPh_3)$_3$] with L^1 or L^2 in toluene at room temperature, the *trans*-chloro hydrido ruthenium complexes *trans*-[RuHC1{η^2-(**L^1** or **L^2**)}$_2$] were synthesized from the reactions of [RuC1$_2$(cod)]$_n$ with L^1 or L^2 in boiling ethanol in the presence of Et_3N. The cyclopentadienyl ruthenium complexes of

diphosphazanes were prepared by the reactions of $[CpRu(PPh_3)_2C1]$ with chiral or unsymmetrical diphosphazanes in boiling toluene for 5 hours.

The sulfur monocapped ruthenium complexes $[Ru_3(\mu_3\text{-}S)(\mu\text{-}CO)(CO)_7\{\eta^2\text{-}(Ph_2PN(R)PPh_2)\}]$ were prepared by the reactions of $[Ru_3(CO)_{12}]$ with L^1S or L^2S in the presence of $Me_3NO.2H_2O$ in boiling toluene. The rhodium (**I**) complexes prepared by the reactions of $[Rh(cod)_2]BF_4$ or $[Rh(\mu\text{-}C1)(CO)_2]_2$ with L^1S or L^2S in benzene at room temperature.

Treatment of $[ReOC1_3(PPh_3)_2]$ with $Ph_2PN(R)PPh_2$ (R=(*S*)-*CHMePh or $CHMe_2$) in toluene medium gives rhenium(V) complexes bearing diphosphazane monoxide ligand $[ReOC1_3\{\eta^2\text{-}(Ph_2PN(R)P(O)Ph_2)\}]$ (**8**) (R=(*S*)-*CHMePh or $CHMe_2$). The reaction between Re_2O_7 and $Ph_2PN(CHMe_2)$ PPh_2 in dry dichloromethane at -45^OC gives $[ReO_2\{\eta^2\text{-}(Ph_2PN(R)PPh_2)\}_2]ReO_4$.

The unsymmetrical diastereomeric diphosphazanes $X_2PN(R)PYY'$ (X=Ph, R=(*S*)-*CHMePh, YY' = (*R*),(*S*)-$O_2C_{20}H_{12}$ were prepared by the reaction of the chiral aminophosphane Ph_2PNH(*S*)-*CHMePh) with racemic [1,1'-binapthyl]-2,2'-phosphorochloridite (*S*),(*R*)-$CIP(O_2C_{20}H_{12})$ in the presence of triethylamine. The reaction of $[PdC1_2(cod)]$ with 1:1 molar proportion of (*SR*),(*SS*)-$Ph_2PN(R)P(O_2C_{20}H_{12})$ (R=(*S*)-*CHMePh) in dichloromethane at room temperature gives the diastereomeric complexes (*SR*),(*SS*)-$[PdC1_2\{\eta^2\text{-}(Ph_2PN(R)P(O_2C_{20}H_{12}))\}]$. One of the diastereomers (SR) is isolated in a pure state by selective crystallization from CH_2C1_2/petrol (1:1).

The general procedure for asymmetric hydrogenation is as follows: Itaconic acid and the ligand were dissolved in 20 ml of deoxygenated CH_3OH/toluene (3:1) mixture. The solution was purged with hydrogen gas and the catalyst $[RhC1(cod)]_2$ was added and the mixture was stirred at 25^OC for 4–5 days. The solvent was removed *in vacuo* to obtain methylsuccinic acid. Optical rotation was measured for the methylsuccinic acid and the enantiomeric excess (e.e) was calculated.

4. Summary

Several new rhenium, ruthenium, rhodium and palladium complexes of chiral and unsymmetrical diphosphazanes have been synthesized and their structure elucidated by NMR spectroscopy and X-ray crystallographic studies. A novel synthetic strategy has been developed for a series of 'chiral-at-metal' half-sandwich ruthenium complexes of diphosphazanes. Reactions of $Ru_3(CO)_{12}$ with diphosphazane monosulfides provide a facile route for monocapped chiral clusters. Only a modest level of asymmetric induction is observed in the asymmetric hydrogenation reactions using rhodium complexes of diphosphazanes and diphosphazane monosulfides. There is considerable scope for further tuning the diphosphazane ligands to enhance the enantiomeric excess and studies in this direction will be rewarding.

References

1. Balakrishna, M. S., Reddy, V. S. Krishnamurthy, S. S., Nixon, J. F. and Burckett St. Laurent, J. C. T. R. — *Coord. Chem. Rev.*, 1994, **129**, 1.

2. Witt, M. and Roesky, H. W. — *Chem. Rev.*, 1994, **94**, 1163.

3. Bhattacharyya, P. and Woollins, J. D. — *Polyhedron*, 1995, **14**, 3367.

4. KRISHNAMURTHY, S. S. *Proc. Indian. Acad. Sci. (Chem. Sci.,)* 1996, **108**, 111.

5. BABU, R. P. K., KRISHNAMURTHY, S. S. AND NETHAJI, M. *Tetrahedron: Asymmetry,* 1995, **6**, 427.

6. CROSS, R. J., GREEN, T. H. AND KEAT, R. J. *J. Chem. Soc., Dalton Trans.,* 1976, 1424.

7. BABU, R. P. K., APARNA, K. KRISHNAMURTHY, S. S. AND NETHAJI, M. *Phosphorus, Sulfur Silicon,* 1995, **103**, 39.

8. BABU, R. P. K., KRISHNAMURTHY, S. S. AND NETHAJI, M. *Heteroatom. Chem.,* 1991, **2**, 477.

Thesis Abstract (Ph.D.)

Host–parasite interaction in heme biosynthesis by the malarial parasite. Identification of a novel drug target in the parasite by Zahid Quyoom Bonday
Research supervisor: Prof. G. Padmanaban
Department: Biochemistry

1. Introduction

Although malaria is no longer a threat in most temperature, advanced areas of the world, it still persists as a major health problems for close to a billion people visiting or residing in the tropics and less-advanced subtropical areas. Despite extensive control efforts, the incidence of the disease is not decreasing in most malaria-endemic areas of the world and in some it is clearly increasing. With the recongnition of deficiencies in control programs based on insecticides and antimalarial vaccines, drugs have acquired importance as a frontline control measure against malaria. This increased reliance upon drugs in hampered by two important limitations: a) no single compound is suitable for all purposes, and b) the efficacy of available drugs suffers from the widespread, and alarmingly increasing, occurrence of drug-resistant parasites. These factors highlight the need for new antimalarial drugs, ideally directed against new targets. Potential targets for chemotherapy include those that are present in the parasite and absent in the human host, and those that are present in both the parasite and its human host, but differ sufficiently to allow the synthesis of parasite-specific drugs. The latter group of targets includes the various metabolic pathways of the malaria parasites, many enzymes of which offer tremendous scope for the development of novel drugs. The present work deals with one such aspect, namely, heme biosynthesis in the malarial parasite. With the aim of evaluating its potential as a drug target, a detailed investigation of the heme biosynthetic pathway in the parasite was carried out.

2. Materials and methods

All chemicals and enzymes were purchased from Sigma Chemicals (USA), Bangalore Genei (India), Merck (Germany), and Qualigens (India). ALAD cDNA and ALAS antibodies were kind gifts from Dr Terry Bishop and Dr Gloria Ferriera, respectively.

ALAD, ALAS and ferrochelatase were assayed in parasite and RBC fractions according to standard protocols. For purifying ALAD from the parasite fractions, DEAE Sephacy1, Pheny1 Sepharose, Octy1 Sepharose and Sepharose CL-4B were used. Immunogold electron microscopy

was carried out in Dr P. D. Gupta's Laboratory. Reticulocytes were stained with methylene blue and for DNA staining Hoechst stain was used.

3. Results and discussion

The mouse and human malarial parasites, *Plasmodium berghei* and *Plasmodium falciparum*, respectively, synthesize heme *de novo* following the standard pathway observed in animals. Malarial parasite requires heme for optimal protein synthesis and dies if its heme biosynthesis is inhibited. The present study on the heme biosynthetic pathway of the malarial parasite revealed certain interesting features. The isolated parasite has low levels of δ-aminolevulinate dehydratase (ALAD), second enzyme of the pathway, and the data clearly indicated it to be of red cell origin. The purified enzyme preparation from the uninfected red cell and *P. berghei* were identical in kinetic properties, subunit molecular weight, cross-reaction with antibodies to the human enzyme, and N-terminal amino acid sequence. Immunogold electron microscopy of *P. berghei* indicated that the enzyme is present inside the parasite and, therefore, was not an experimental contaminant. Thus, the parasite derives or imports ALAD from the host.

A number of results provide support for the import hypothesis: i) A 65 kDa ALAD-binding protein, having a high affinity for ALAD, was detected on the plasma membrane of *P. berghei*. The binding of ALAD to the parasite membrane protein was seen to be pH dependent with the binding being maximum at pH 6.5. ii) Domain mapping experiments indicated that the central region of ALAD retains the capacity to bind to the parasite membrane and also inhibits the binding of full-length ALAD to the membrane protein. Incubation of *P. falciparum* cultures with this particular domain of ALAD leads to an impairment in the import of functional ALAD from the host erythrocytes into the parasites, thereby causing inhibition of heme synthesis in the parasites and hence their death. iii) Irreversible inhibition of host erythrocyte ALAD resulted in a corresponding inhibition of ALAD in the parasite. It could, therefore, be concluded that the parasite imports ALAD from the host to synthesize heme *de novo*. In contrast, δ-aminolevulinate synthase (ALAS), the first enzyme of the pathway, in the parasite behaves differently from that of the host erythrocytes so for as cross-reactivity with antibodies against the human ALAS is concerned, thus indicating that the parasite has a unique species of ALAS.

A detailed examination of ALAD activity, protein and mRNA in the infected red blood cells of mice revealed that parasite (*P. berghei*) infection leads to a dramatic increase in their levels in the erythrocytes. The induction in ALAD is intrinsic to infected red blood cells and this is intriguing in view of the fact that mature erythrocytes, which comprise more than 95% of red cells in the blood, are transcriptionally and translationally incompetent. So to provide an explanation for the observed increase in ALAD in the blood of infected mice two possibilities were considered: a) Malarial parasites bring about a large-scale destruction (hemolysis) of host erythrocytes. The consequent host response leads to the release of reticulocytes into the peripheral blood. Since reticulocytes are enriched in RNA and are capable of translation, it is possible that the increased ALAD message and protein in the blood of infected mice owes its origin to parasite-induced hemolytic anemia and hence the elevated reticulocyte percentage in the blood. However, arguing against this possibility are the observations that: i) reticulocyte numbers in the peripheral blood do not increase till the fifth day of infection although induction of ALAD message in the infected red blood cells is notable by the third day and are significant by the fourth day of infection. ii)

Hemolytic anemia brought about by 1-acety1-2-phenyl-hydrazine (APH), a commonly used hemolytic agent, leads to a concomitant increase in ALAS and ALAD in the blood of such mice. On the other hand, no increase at all was observed in ALAS message or protein in the blood of *P. berghei*-infected mice. b) In contrast to reticulocytes, significant number of nucleated early-erythroid stages become evident in the blood of *P. berghei*-infected mice by the third day of infection, which correlates well with the augmentation of ALAD levels in the infected blood. It seems possible that increased ALAD levels seen in the infected blood owe their origin to these cells. However, more experimentation is needed before this aspect is confirmed.

In conclusion, it can be seen that the import of host erythrocyte ALAD into the malarial parasite is vital for parasite heme biosynthesis and the machinery involved in bringing about this import is a novel drug target. In addition, ALAS of the parasite, which appears to be different from that of the host species, may be another potential drug target. At the other end of the spectrum, the concomitant appearance of nucleated erythroid cells and increased ALAD message and protein in the blood at an early stage during *P. berghei*- infection of mice raises the interesting question whether such cells are the preferential candidates for *P. berghei* infection.

References

1. Fujioka, H. and Aikawa, M. — *Expl Parasitol.*, 1993, **76**, 302–307.
2. Gabay, T. and Ginsburg, H. — *Expl Parasitol.*, 1993, **77**, 261–272.
3. Galinski, M. R. and Barnwell, J. W. — *Am. Trop. Med. Parasitol.*, 1995, **89**, 113–120.
4. Galinski, M. R. and Barnwell, J. W. — *Parasitol. Today*, 1996, **12**, 20–29.
5. Ganguly, N. K., Sandhu, H. Dubey, M. L. and Mahajan, R. C. — *Indian J. Med. Res.*, 1997, **106**, 70–78.
6. Gardner, L. C., Smith, S. J. and Cox, T. M. — *J. Biol. Chem.*, 1991, **266**, 22010–22018.
7. Gardner, M. J., Williamson, D. H. and Wilson, R. J. M. — *Mol. Biochem. Parasitol.*, 1991, **44**, 115–124.
8. Gardner, M. J. *et. al.* — *Gene*, 1994, **144**, 307–308.
9. Garnham, P. C. C. — In *Malaria*, Vol. 1, (Kreir, J. P. ed.), Academic Press, 1980, pp. 96–144.
10. Gaughan, P. L. Z. and Krassner, S. M. — *Comp. Biochem. Physiol. B*, 1971, **39**, 5–18.
11. Geary, T. G., Jensen, J. B. and Ginsburg, H. — *Biochem. Pharmacal.*, 1986, **35**, 3805–3812.

Thesis Abstract (Ph. D.)

***Bombyx mori* Nucleopolyhedrosis virus: Expression from very late promoters** by S. Sriram
Research supervisor: Prof. K. P. Gopinathan
Department: Molecular and Cellular Biology

1. Introduction

Baculovirus expression system has been widely used to produce soluble, post-translationally processed recombinant proteins in biologically active form. For high-level expression of the cloned foreign genes, the promoters of the hyper transcribed very late genes, *polyhedrin* (*polh*) and *p10* from the virus are mainly utilised. *Autographa californica* nucleopolyhedrosis virus (AcMNPV) has been most extensively exploited followed by *Bombyx mori* nucleopolyhedrosis virus (BmNPV) for expression in permissive insect cell lines. Both these viruses share about 90% homology at DNA level but they differ in their host range. Many proteins have been over-expressed in insect cell lines using the prototype AcMNPV system.[1] The BmNPV system offers an economically viable alternative for high-level expression through the larval catterpillars. High-level expression of biologically active proteins and easy methods for protein isolation from the recombinant BmNPV-infected silkworm larvae have been documented.[2]

2. Results and discussion

2.1. *Expression from AcMNPV very late promoters in Bombyx-derived cells and generation of recombinant BmNPVs by homeologous recombination*

Although many proteins have been expressed to high levels in silkworm larvae, the major handicaps of the BmNPV system have been the limited availability of transfer vectors for optimised expression and the absence of simplified recombinant virus selection procedures. Attempts were made to examine whether the currently available large collection of AcMNPV-based *polh* and *p10* vectors are functional in BmN cells infected with BmNPV using *luciferase* (*luc*) as a reporter gene. The heterologous promoters, *polh* and *p10*, from AcNPV function as efficiently in BmN cells as the BmNPV promoters. The location of the cloned foreign gene with respect to the promoter sequences was important for achieving the highest levels of expression which followed the order +35 > –3 > –8 nucleotides (nt) with respect to the *polh* start codons.

Both AcMNPV and BmNPV showed high overall homology at the *polh* and *p10* loci. Taking advantage of this, homeologous recombination between AcMNPV-based *polh* and *p10* transfer vectors and BmNPVs viral DNA were attempted. Recombinant BmNPV harbouring *luc* in both *polh* and *p10* promoters were successfully generated. High levels of luciferase expression were observed in BmN cells as well as *B.mori* larvae infected with recombinant BmNPV-harbouring luciferase gene under the AcMNPV *polh* and *p10* promoters. The homeologous recombination approach facilitated the direct exploitation of currently available, varied collection of second-generation AcNPV *polh* and *p10* transfer vectors without further modifications in the BmNPV system.

2.2. *Cloning and characterization of lef2 from BmNPV*

The molecular mechanisms governing high levels of transcription from the very late promoters is poorly understood. So far, 18 virally encoded late gene expression factors (Lefs) have been identified to be necessary and sufficient for late gene expression from AcMNPV[3] but their molecular basis of action is not well established. The positions of Lef homologues in BmNPV genome are shown in Fig 1.

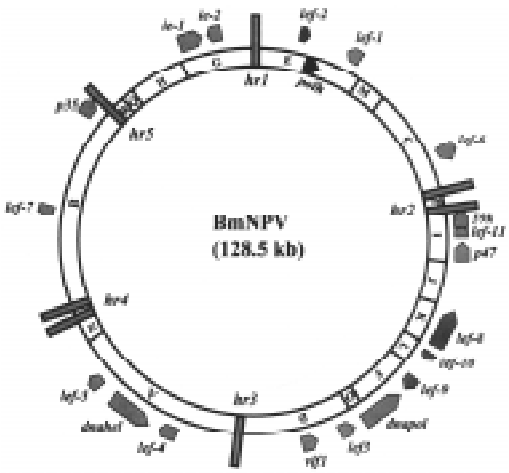

Fig. 1. Ciruclar map of BmNPV genome. Positions of the 18 lefs, identified based on sequence comparison with AcMNPV, are indicated on the physical map based on *Eco*RI restriction pattern.

The *late gene expression factors* 2 (*lef2*) from BmNPV encoding an ORF of 209aa was identified based on sequence homology to the AcMNPV counterpart and was cloned by PCR amplification from the viral genomic DNA. This gene has been characterized here in detail in terms of its temporal expression and its role in viral DNA replication and transcription.

The temporal transcription profiles of *lef2* revealed the presence of a 1.2 kb transcript in both delayed early and late periods following virus infection. Transcription start site mapping identified a late promoter at –352 nt (TAAG) and an early promoter at –312 nt (TTGT) from the +1 ATG of *lef*2. In order to study the expression of *lef2* in BmN cells infected with BmNPV, Lef2 was synthesized as a GST fusion protein in *E.coli* and polyclonal antibodies were raised. A 24kD protein corresponding to Lef2 was detectable in BmNPV-infected BmN cells at 48 h post infection. This protein was localized both in the nucleus and cytoplasm of the infected cells. In the nucleus Lef2 was specifically associated with the virogenic stroma.

2.3. *Functional role of BmLef2*

In transient expression assays, BmLef2 *trans*-activated very late gene expression from both *polh* and *p10* promoters. An internal deletion encompassing the C-terminal Cys-rich domain abolished the transcriptional activation from *polh* promoter. The enhanced expression from very late promoters in the presence of Lef2 could be a direct effect on very late gene transcription or due to an indirect effect by increasing viral DNA replication. This aspect was examined in detail by delineating replication and transcription events by specifically inhibiting the function of *lef2* either prior to DNA replication or following DNA replication by expressing antisense transcripts to *lef2* under immediate early (*ie-1*) and *polh* promotes. Inactivation of Lef2 synthesis at late periods drastically reduced the very late gene transcription but showed little effect on DNA replication. On the other hand, the presence of antisense lef2 at early times caused 45–50% reduction in viral titers as well as 55–60% inhibition of the viral DNA synthesis. Further, a direct effect of *lef2* on plasmid-based DNA replication in virus-infected cells (mediated by *viral hr* sequences) was also demonstrated. Thus Lef2 exhibited a dual function in viral DNA replication as very late gene *transcription*.

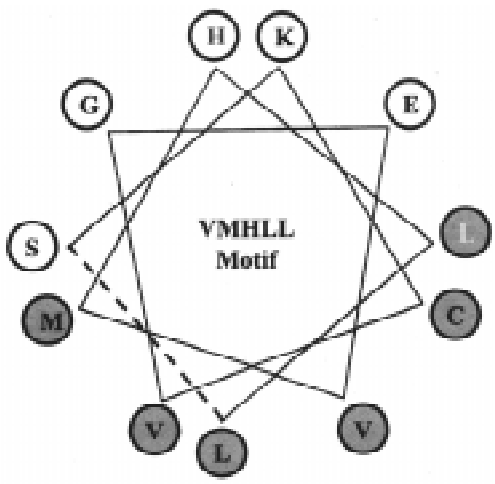

Fig. 2. Amphipathic helix of the VMHLL motif in Lef2. The helical wheel of a-helical region encompassing the VMHLL motif (163–173 aa). The presence of hydrophobic amino acids on one side (white circles) and hydrophilic residues on the other (gray circles) are evident.

The role of Lef2 in very late gene expression was investigated in greater detail. The C-terminal Cys-rich region showed weak homology to the CH3 domain of the mammalian transcription activator p300. Possible association of Lef2 with other viral or host proteins involved in very late gene transcription was investigated by co-immunoprecipitations with antiLef2 antibodies. Lef2 was associated with three proteins of 31, 35 and 38 kD. Possible interaction of Lef2 with TBP (38 kD) was therefore tested by co-immunoprecipitations with antiTBP antibodies. The 24 kD band corresponding to Lef2 was detectable in co-immunoprecipitations with antiTBP antibodies. The interaction between Lef2 and TBP was further confirmed by TBP-agarose pull downs using radiolabelled Gst-Lef2. These results suggest that Lef2 could be acting as a transcriptional co-activator.

A leucine-rich LXXLL motif present in the N-terminal region of p300/CBP and in family of nuclear receptors is known to mediate protein–protein interaction.[4] Two similar motifs, LYMLL (at aa 57) and VMHLL (at aa 19) were identified in Lef2. The amphipathic α-helical region formed by the LYMLL motif is shown in Fig. 2. The effect of mutating the invariant leucines on late gene transcriptional activation was studied in a mutant Lef2 background. A point mutation of D178 in (AcMNPV) *lef2* has been previously shown to affect very late gene expression.[5] A similar mutant virus of AcMNPV (Lef2 D178G) was therefore generated here in order to test the effect of various mutations of the VMHLL motif of Bm*lef2*, in transient transfection assays. Infection with the *lef2* mutant AcMNPV (D178G) resulted in very low expression from the very late promoters (*polh* and *p10*) which was restored to high levels by cotransfection with wild-type Bm*Lef2*. However, the transcription from *polh* promoter was not stimulated once the VMHLL or LYMLL motifs were mutated. These studies revealed that the highly conserved residues are essential for mediating very late gene expression by Lef2. Thus, Lef2 plays a direct role in very late gene expression by acting as a transcriptional co-activator.

References

1. O'Reilly, D. R., Miller, L. K. and Luckow, V. E. *Baculovirus expression vectors. A laboratory manual*, W. H. Freeman, 1992.

2. Palhan, V. B., Sumathy, S. and Gopinathan, K. P. *Bio/Techniques*, 1995, **19**, 97–104.

3. Todd, J. W., Passarelli, L. A., Lu, A. and Miller, L. K. *J. Virol.*, 1996, **70**, 2307–2317.

4. Heery, D. M., Kalkhoven, E., Hoare, S. and Parker, M. G. *Nature*, 1997, **387**, 733–735.

5. Merrington, C. L., Kitts, P. A. King, L. A. and Possee, R. D. *Virology*, 1996, **217**, 338–348.

Thesis Abstract (Ph. D.)

Preparation of M-β-aluminas (M = Li, Na, K, Rb, Or, H^+) by soft chemistry methods and thier characterisation by V. Jayaraman
Research supervisor: Prof. T. R. N. Kutty
Department: Materials Research Centre

1. Introduction

Ion-conducting β-alumina is a class of solid electrolyte compounds with general formula $M_2O.xAl_2O_3$, where M is typically Na, K, Li, Rb, Ag, H^+, $NH4^+$, Tl^+, etc. and where x varies from 5 to 11. The two subgroups of this class of compounds are: 1) β-phase comprises M_2O: AL_2O_3 = 1:8–1:11 and β"-phase comprises M_2O: AL_2O_3 = 1:5–1:7. These aluminates possess a characteristic layered structure consisting of spinel blocks linked together by oxygen and alkali ions (typically) in loosely packed layers. Because of the characteristic layered structure with high mobility of ions[1] present in the inter-block layer, these compounds find use in various technological applications such as secondary batteries, fuel cells, thermoelectric converters, sensors, etc. Hence, a large amount of research and developmental activities are being pursued on these compounds. For all the applications mentioned above, β-alumina products with good ionic conductivity and density are required. The conventional method for large scale production of these compounds involves high temperature reactions of β-alumina with Na_2CO_3 in the presence of small quantities of Li_2O or MgO as the stabiliser. As high temperature is involved, significant soda loss occurs which results in reduced conductivities of the products. Also, sintering of the prepared powders is done at even higher temperatures; extensive grain growth persists and consequently, results in poor mechanical properties of the shaped products. The starting materials are mechanically mixed using a mortar and pestle or a planetary mill which introduces impurities on repeated use. These impurities will introduce significant electronic conductivity if they exhibit variable valency. To overcome these limitations, different methods of preparation such as co-precipitation, spray-freeze drying and sol–gel techniques are attempted for the preparation of β-alumina. Also, these methods aim to significantly bring down the reaction temperature between the constituents and the sintering temperature. The present investigation has been undertaken to synthesise various β-aluminas by a novel get-to-crystallite conversion method and characterise them. The various preparative parameters are identified and optimised for all the β-aluminas prepared. Stability ranges of some of the β-aluminas are studied and the extended stabilities of them are explained. Novel ion exchange procedures are employed for the preparation of lithium and proton-β-aluminas.

2. Experimental techniques

The principles involved and the experimental details of G-C conversion technique and hydrothermal methods are presented in our publications.[2–6] The chemical compositions of the products were determined by the wet chemical analyses using atomic absorption spectroscopy (AAS). Thermal analyses were performed on a simultaneous thermogravimetry–differential thermal analysis (TG/DTA) instrument from Polymer Laboratory STA–1500 at a heating rate of $5^{O}C$/min. Phase identification of the powders was carried out by X-ray powder diffraction using Siemens D 500 model diffractometer. Infrared absorption spectra were recorded on a BOMEM spectrometer in the range 4000–400 cm^{-1}. Solid-state ^{27}Al MAS NMR spectra were obtained at 78.2 MHz using a high-resolution NMR spectrometer (Bruker 300 MHz) at room temperature fitted with a magic angle spinning probe (MAS) for rotating the sample at a frequency of 7 kHz. ^{27}Al MAS NMR chemical shifts (δ) were referenced to 1M $A1(H_2O_2)_6Cl_3$ solution having the assigned $\delta = 0$. High-resolution electron microscopy (HREM) was carried out using JEOL-JEM 200 CX transmission electron microscope (TEM) operating at 200 kV and equipped with ultra-high-resolution objective pole-piece in the top-entry configuration.

3. Results and discussion

Coarse gels of hydrated alumina $A1_2O_3$. yH_2O ($80< y <120$) were reacted with sodium hydroxide solution in ethanol, which yielded crystalline $Na_xA1O_x(OH)_{3-x}$ ($0.17< x <0.23$) having the gibbsite structure with inserted sodium ions (Na-gibbsite). Thermal decomposition of Na-gibbsite above 573 K yielded Na-boehmite intermediate ($Na_xA1O_{1+x}(OH)_{1-x}$). At higher temperatures this intermediate gave rise to Na-γ-alumina and $NaA1_{7/3}O_4$ with a defect spinel structure. It is suggested that because of the cubic close packing of oxygen ions present in the intermediate γ-alumina, formation of Na-β"-alumina takes place above 1273 K as a continuous solid-state process with minimal rearrangement of the close packed oxide ions.[2] The β"-alumina phase thus formed is free of intergrowths of the β-phase, as revealed by HREM and it is stable up to near-melting conditions. A detailed investigation has been undertaken regarding the influence of preparative parameters on the precursor phases formed.[2-3] Depending on the initial concentration of alkali used, the precursor phase that crystallised can be varied from Na-pseudoboehmite to a mixture of Na-gibbsite and Na-bayerite through Na-gibbsite. At lower alkali to alumina ratios ($Na_2O/A1_2O_3<0.31$), Na-pseudoboehmite precursor is stabilised, at intermediate ratios ($Na_2O/A1_2O_3 = 0.31–0.60$) Na-gibbsite is stabilised and above the $Na_2O/A1_2O_3$ ratio of 0.60, Na-bayerite precursor is also stabilised along with Na-gibbsite. On calcination, Na-pseudoboehmite gives rise to α-alumina along with Na-β-alumina, whereas Na-gibbsite precursor yields phase-pure Na-β"-alumina. When the ethanol–water composition (solvent ratio) was maintained around 2, a mixture of Na-gibbsite and bayerite is obtained for a ratio of $Na_2O/A1_2O_3$=0.70, and when the ratio was raised to 4, phase-pure Na-gibbsite is obtained. Na-gibbsite together with Na-pseudoboehmite crystallised at higher solvent ratios. It is observed that the nonaqueous solvents destabilise the gel irreversibly in the presence of alkali hydroxide by decreasing the effective ionic pressure within the gel cavities, and at the same time prevent the back diffusion of alkali ions inserted within the precursor lattice. In the presence of the strongly desiccative (water attractive) solvents, dehydroxylation of Na-gibbsite takes place under wet chemical conditions to yield Na-pseudoboehmite. It is also observed that irrespective of the duration of aging of gels, the precursor phase remains the same for a given solvent and hence the final product phase.

Density of 97% (TD) was obtained on sintering of the compacted disks at 1923 K. Conductivity values of the sintered samples were around 0.1 S cm^{-1} at 573 K.

Hydrated alumina gel yields K-pseudoboehmite or K-gibbsite on reaction with alcoholic KOH in the preparation of potassium-β/β''-aluminas by G-C conversion method. Thermal decomposition of these precursors above 500 K yielded K-boehmite. Above 1473 K, K-β-alumina was obtained via a modified K-χ-alumina intermediate. To obtain K-β''-alumina, Li^+ or Mg^{2+} is incorporated which yields K-γ-alumina intermediate on heating the precursor, K-gibbsite, above 723 K. Above 1473 K, phase-pure K-β''-alumina was obtained on heating K-γ-alumina intermediate. K-β''-alumina is also obtained by heating K-pseudoboehmite or K-gibbsite precursor with excess K_2CO_3 above 1473 K. When the initial ratio of reactants ($K_2O/A1_2O_3$) was varied from 0.15 to 0.77, K-pseudoboehmite was obtained as the precursor phase and above this ratio, K-gibbsite was obtained as the precursor. The maximum amount of potassium inserted in the precursor phase corresponds to the $K_2O/A1_2O_3$ ratio of 0.135, which is much lower than the ratio observed with the preparations involving sodium hydroxide in which the amount of sodium ions inserted in the precursor corresponds to a $Na_2O/A1_2O_3$ ratio of 0.195. Thus, as the ionic size increases, the amount of alkali ion inserted into the precursor decreases. The precursors, either K-pseudoboehmite or K-gibbsite, yielded only K-β-alumina on calcining at 1473 K as the concentration of potassium inserted is not sufficient to stabilise K-β''-alumina phase. As the solvent ratio is decreased from 2 to 1.3, the amount of potassium inserted also decreases which alters the K_2O:$A1_2O_3$ ratio from 1:12 to 1:17 with the retention of the same precursor phase. On calcination of this precursor phase yields K-β-alumina. This shows that the stability range of K-β-alumina can be extended up to 1:17 by the present method. The extended compositional range of stability of K-β-alumina is explained on the basis of the polysynthetic lamellae arising from the collapse of the layers adjacent to the K-O plane, as revealed by HREM. The increased number of $A1O_6$ octahedra, in comparison to $A1O_4$ tetrahedra and the prevalence of distorted $A1O_6$ with two or more types of second nearest neighbour interaction is indicated from the solid-state ^{27}Al MAS NMR studies.[4]

Li-β''-alumina is prepared by a heterogeneous ion-exchange reaction[5] between Na-β''-alumina and LiC1 in the solid state or melt at 800 to 930 K. Earlier, it was reported in the literature that ion exchange with lithium chloride melt is very difficult and little lithium is exchanged for sodium.[6] The high degree of exchangeability of sodium with lithium is attributed to the high reactivity of the reactant, Na-β''-alumina, obtained from the wet chemical gel-to-crystallite conversion technique. High-resolution transmission electron microscopy revealed the presence of splinter fragments resulting from high density of stacking faults in Li-β''-alumina. Thermal stability studies on Li-β''-alumina showed the intradiffusion of Li^+ ions from the conduction planes into the spinel blocks above 1073 K leading to the formation of γ-$LiA1O_2$ and $LiA1_5O_8$, which on further heating to 1673 K gave rise to lithium aluminospinel, $LiA1_5O_8$ as a result of Li_2O evaporation. Preparation of lithium-β/β''-aluminas has also been attempted through novel wet chemical method, viz. gel-to-crystallite conversion method and hydrothermal method.[7] In the gel-to-crystallite conversion method, on reaction of hydrated alumina gel with alcoholic LiOH yielded layered double hydroxide (LDH) with chemical composition $LiA1_2(OH)_7$. $2H_2O$ as precursor which on calcination yielded lithium aluminospinel, $LiA1_5O_8$ at 1673 K. In the hydrothermal method, the precursor obtained was either the layered double hydroxide at lower temperatures (413 K) or γ-A1OOH at higher temperatures (523 K) of reaction. These precursors yielded

lithium aluminospinel on calcination at 1673 K irrespective of the initial concentration of LiOH used in the reaction. Also, large amounts of lithium ions are inserted in the precursor matrix which correspond to an $Li_2O/A1_2O_3$ ratio of ~ 0.5. The increased concentration of lithium ion insertion is attributed to its small size. The formation of aluminospinel phase from the wet chemical methods has been rationalised as follows: lithium ion being a hard acid, prefers to occupy the highest coordination site, thus forms LiO_6 octahedra in the aluminospinel lattice instead of occupying the conduction plane in the β-alumina structure.

The only earlier report[8] on the preparation of rubidium-β-alumina was by a solid-state reaction of α-alumina with Rb_2CO_3 at 1573 K, which reported the absence of the characteristic (002) reflection of β-alumina system and the product was identified as 'β-alumina type'. Hence, the preparation of this compound is attempted by gel-to-crystallite conversion method. Irrespective of the initial ratio of the reactants used in the wet chemical preparation, the precursor phase stabilised was Rb-pseudoboehmite and the maximum concentration of Rb^+ ions inserted in the precursor phase corresponds to a $Rb_2O:A1_2O_3$ ratio of 1:21. The present studies showed that the stability range of Rb-β-alumina can be extended up to 1:22. The extended compositional range of stability of Rb-β-alumina is accounted for in terms of the changing pattern of stacking layers of the spinel blocks from HREM studies. The decreased concentration of Rb^+ ions in the conduction planes is balanced by the changing widths of spinel blocks of formula, $(A1_{11}O_{16})^+$ which is charge balanced by the adjoining $[Rb(A1_{10}O_{16})]^-$. Double or triple layers of such change compensative pairs $(A1_{11}O_{16})^+[Rb(A1_{10}O_{16})]^-$ have been proposed for stabilising Rb-β-alumina structure with lower concentrations of rubidium.[9]

A novel ion exchange procedure under hydrothermal conditions using dilute acetic acid or dilute sulphuric acid for the preparation of proton-β/β''-alumina is adapted for the first time.[10] The temperatures involved in this process are found to be 423 to 438 K and the durations involved are 2 to 10 h normally. Using this procedure, the conditions for the preparation of proton-β/β''-aluminas using acetic acid and sulphuric acid have been optimised. Also, the simplicity of this procedure is demonstrated by ion exchanging sodium ions in Na-β-alumina with proton which is difficult to achieve otherwise. The new method offers the tunability for the preparation of a range of proton-β/β''-aluminas from $H_2O:A1_2O_3 = 1:5$ to $H_2O:A1_2O_3 = 1:17$ by properly choosing the initial precursor for the ion exchange reaction. Thus, the stability range of proton-β-alumina is established up to $H_2O:A1_2O_3$ ratio of 1:17. The stability of proton-β-alumina under high pressures and temperatures is also envisaged. At high pressures under hydrothermal conditions, transformation of the initially formed proton-β-alumina phase to boehmite phase was observed. It is proposed that under high pressures, concomitant to the loss of hydroxonium ions from the lattice, the layered structure with small concentrations of hydroxonium ions collapses and rearranges to a more stable boehmite structure. When proton-β-alumina is subjected to temperatures as high as 1273 K, all the hydroxonium ions present in the conduction plane are driven out which leads to the rearrangement of the β-alumina structure to corundum (α-alumina) structure. Also proton-β-alumina is found to be stable up to a temperature of 723 K which is attributed to the novel hydrothermal procedure employed for its preparation.

References

1. KUMMER, J. T. *Prog. Solid St. Chem.*, 1972, **7,** 141.

2. KUTTY, T. R. N., JAYARAMAN, V. AND PERIASWAMI, G. — *Mater. Res. Bull.,* 1996, **31,** 1159.

3. JAYARAMAN, V., PERIASWAMI, G. AND KUTTY, T. R. N. — *Mater. Chem. Phys.,* 1998, **52,** 46.

4. KUTTY, T. R. N., JAYARAMAN, V. AND PERIASWAMI, G. — *J. Mater. Chem.,* 1998, **8,** 1087.

5. JAYARAMAN, V., PERIASWAMI, G. AND KUTTY, T. R. N. — *Mater. Res. Bull.,* 1998, **33,** 1811.

6. CLEARFIELD, A. — *Chem. Rev.,* 1988, **88,** 125.

7. NAYAK, M., KUTTY, T. R. N., JAYARAMAN, V. AND PERIASWAMI, G. — *J. Mater. Chem.,* 1997, **7,** 2131.

8. VERSTEGEN — Philips, Eindhoven, Netherlands, Private communication.

9. JAYARAMAN, V., PERIASWAMI, G. AND KUTTY, T. R. N. — *Mater. Res. Bull.,* 2000, **35,** 1213.

10. KUTTY, T. R. N., JAYARAMAN, V. AND PERIASWAMI, G. — *Solid St. Ionics,* 2000, **128,** 161.

Thesis Abstract (Ph. D.)

Electron spectroscopic investigations of gas–solid interactions and bimetallic clusters by K. R. Harikumar
Research supervisor: Prof. C. N. R. Rao
Department: Solid State and Structural Chemistry Unit

1. Introduction

This work is primarily concerned with the study of the interaction of carbon monoxide and alcohols with surfaces of model Cu/ZnO catalysts or zinc as well as with the study of bimetallic clusters. It comprises three parts. Part 1 describes the interaction of carbon monoxide and methanol with model Cu/ZnO catalyst surfaces. Part 2 consists of a study of C-O bond scission of alcohols on polycrystalline and (0001) surfaces of zinc. Part 3 comprises investigations of bimetallic clusters. In all these investigations, X-ray photoelectron spectroscopy and related surface spectroscopic techniques have been employed.

2. Experimental

ZnO substrates were prepared *in situ* by surface oxidation of high-purity (99.9%) polycrystalline zinc foils from Johnson–Matthey in the preparation chamber of the spectrometer. The polycrystalline foils were cleaned *in situ* in the sample preparation chamber of the instrument by Ar^+ ion etching and annealing unit clean surfaces, devoid of carbon and oxygen, were obtained. ZnO films of various thicknesses were prepared *in situ* by controlled oxidation of an atomically clean Zn surface. Oxygen exposures are given in langmuir. The development of the ZnO layers was followed by means of variation of the Zn(LMM) Auger spectrum at different oxygen exposures

and temperatures. The thickness of the ZnO layer was determined by using the equation

$$I = I_0 \exp(-d/\lambda),$$

where I_0 and I are the intensities of the Zn^0(LMM) Auger signal before and after oxidation, respectively, λ is the escape depth in the oxide and d the thickness of the oxide layer. The thickness of the oxide layers obtained by exposing the foil at 10^5L oxygen pressure at 300 K is 5 Å. The 10 Å ZnO layer could be obtained by heating the Zn foil at 450 K for about 30 min in O_2 atmosphere (1 atm).

Cu clusters were obtained by the resistive evaporation of high-purity Cu (wound around a thoroughly dagassed tungsten filament) at room temperature under ultra-high vaccum conditions in the preparation chamber of the spectrometer. The coverages of Cu were quantified by means of the ratio of the intensity of the Cu($2p_{3/2}$) feature, I_{Cu}, and the intensity of the Zn($2p_{3/2}$) signal of the AnO/Zn substrate, I_{zn}. Alternatively, the surface concentrations, σ, of the deposited metals have been estimated following the method of Carley and Roberts, using the following equations,

$$\frac{I_m}{I_s} = \frac{\mu_m M_s \sigma}{NCos\phi\mu_s\rho\lambda}$$

where I_m and I_s are the integrated photoelectron signals from the relevent subshell of the metal and the substrate. M_s and ρ are the molecular weight and density of the substrate, λ is the escape death in the substrate for the particular subshell photoelectrons, ϕ, the angle of collection (with respect to the sample normal) of the photoelectrons and N, the Avogadro number. Cesium was evaporated on to the ZnO(0001) surface by using a well outgassed SAES getter and the Cs coverage has been estimated using the above cited equation.

Carbon monoxide was prepared by the dehydration of formic acid with conc. H_2SO_4 and purified by passing through KOH tower. Final purification was carried out by passing the gas through a liquid N_2 trap. Methanol was further purified on an UHV gas handling system using several freeze-pump-thaw cycles. Adsorption of methanol was carried out by exposing the surfaces to the vapour at 80 K for a coverage of 15L.

Bimetallic clusters were deposited at room temperature under ultra-high vaccum conditions on amorphous graphite surfaces by means of resistive evaporation. First, we mount an appropriate mixture of the two high purity metals wound around a thoroughly degassed tungsten filament. Then the filament was heated in the preparation chamber of the spectrometer, the metals melted and form an alloy in the filament itself. The resistive evaporation of this alloy loaded filament under ultra-high vaccum conditions gives homogenous alloy clusters of required composition. We take the metal coverage θ to be proportional to the intensity ratio $(I_A + I_B)/I_C$, where I_A and I_B are the core-level intensities of the metals and I_C is the C(1s) intensity of the support. We have used these intensity ratios to describe coverage, θ.

3. Results and discussion

The studies discussed in part 1 of the thesis are primarily concerned with the nature of the surface species produced by the interaction of CO and CH_3OH with Cu/ZnO model surfaces. As

part of these investigations, it was necessary to examine the properties of Cu clusters deposited on ZnO/Zn surfaces and the nature of the interaction of CO with Cu clusters. Copper deposited on ZnO/Zn surfaces was first investigated as a function of Cu coverage by employing X-ray photoelectron and Auger electron spectroscopies (XPS and AES). The 2p core-level binding energy of Cu increases with decreasing metal coverage, the maximum shift observed at the smallest coverage being ~ 0.9 eV. Temperature-dependent studies show that Cu diffuses through the ZnO layer with the rate of diffusion varying with the substrate temperature as well as the oxide layer thickness. The inward diffusion of Cu results in the formation of Cu-Zn alloys.[1] Diffusion kinetic experiments at different temperatures show that the activation energy for diffusion increases with increasing oxide layer thickness.

Interaction of CO with Cu clusters deposited on a ZnO(0001) and ZnO/Zn surfaces has been examined by ultra-violet photoelectron spectroscopy(UPS) and XPS. The interaction is stronger with the small Cu clusters deposited on ZnO/Zn surfaces. Interaction of CO is even stronger with annealed Cu/ZnO/Zn surfaces where Cu-Zn alloy particles are present.[2] CO does not absorb on ZnO/Zn surfaces, but absorbs molecularly on the ZnO(0001) surface. Interaction of CO with Cs clusters deposited on a ZnO(0001) surface has also been investigated by XPS and AES. CO transforms to CO_2^- and CO_3^- when CO is adsorbed on a CS-covered ZnO(0001) surface.

Interaction of CO with the model Cu/ZnO catalyst surfaces prepared *in situ* in the spectrometer has been investigated by XPS. The catalyst surfaces contained different proportions of Cu^{+1} and Cu^0 species as determined by Auger spectroscopy. Besides, chemisorbed CO, CO_2^- and CO_3^{2-} species are found on the catalyst surface, the proportion of CO_2^- and CO_3^{2-} relative to CO increasing with the Cu^{1+}/Cu^0 ratio.[3] This observation is significant to methanol synthesis.

Interaction of methanol with Cu clusters deposited on ZnO films grown on a Zn foil as well as on a ZnO(0001) crystal has been examined by XPS. On clean Cu clusters, reversible molecular adsorption or formation of the methoxy species, CH_3O is observed. However, if the Cu clusters are pretreated with oxygen, both the CH_3O and formate, $HCOO^-$ species are produced. Model Cu/Zno catalyst surfaces containing both Cu^{1+}/Cu^0 species show interesting oxidation properties.[4] On a Cu^0-rich catcalyst surface, only the CH_3O species is formed on interaction with CH_3OH. On a Cu^{1+}-rich surface, however, $HCOO^-$ ion is the predominant species.

Interaction of methanol, ethanol, 2-propanol with polycrystalline as well as (0001) surfaces of Zn has been investigated by phototoelectron spectroscopy and vibrational energy loss spectroscopy. All the alcohols show evidence from the condensed species along with the chemisorbed species at 80 K. With increase in temperature to ~ 120 K, the condensed species desorb leaving the chemisorbed species which decompose to give the alkoxy species. The alkoxy species is produced increasingly at lower temperatures as we go from methanol to 2-propanal, the 2-propoxy species occurring even at 80 K. The alkoxy species undergo C-O bond scission giving rise to a hydrocarbon species and oxygen.[5] The C-O bond cleavage occurs at a relatively low temperature of ~ 150 K. The effect of preadsorbed oxygen is to stabilize the alkoxy species and prevent C-O bond scission. On the other hand, coadsorption of oxygen with the three alcohols favours the formation of the alkoxy species and gives rise to hydrocarbon species arising from the C-O bond scission even at 80 K due to the role of oxygen transients.[6]

Core-level binding energies of the component metals in bimetallic clusters of various compositions in the Ni-Cu, Au-Ag, Ni-Pd and Cu-Pd system having been measured as functions of

coverage or cluster size, after having characterized the clusters with respect to sizes and compositions. The core-level binding energy shifts, relative to the bulk metals, at large coverages or cluster sizes, ΔE_a, are found to be identical to those of bulk alloys. By subtracting the ΔE_a values from the observed binding energy shifts, ΔE, we obtain the shifts, ΔE_c, due to cluster size. The ΔE_c values in all the alloy systems increase with decrease in cluster size. These results establish the additivity of the binding energy shifts due to alloying and cluster size effects in bimetallic clusters.[7] Interaction of CO with Cu-Pd and Ni-Cu alloy clusters been found to be dissociative at high temperatures.[8] The interaction of CO with Cu_5Pd clusters is stronger than $Cu_{10}Pd$ clusters.

References

1. HARIKUMAR, K. R., SANTRA, A. K. AND RAO, C. N. R. — An investigation of the Cu/ZnO/Zn system: evidence for the formation of Cu-Zn alloys by the inward diffusion of Cu, *Appl. Surf. Sci.*, 1996, **93,** 135.

2. HARIKUMAR, K. R. AND SANTRA, A. K. — A comparative study of the interaction of CO with Cu and Cu-Zn alloy clusters, *Solid St. Commun.*, 1996, **99**, 403.

3. HARIKUMAR, K. R. AND RAO, C. N. R. — Interaction of CO with Cu/ZnO catalyst surfaces prepared *in situ* in the electron spectrometer: Evidence for CO_2^- and related species relevant to methanol synthesis, *Appl. Surf. Sci.*, 1998, **125**, 245.

4. HARIKUMAR, K. R. AND RAO, C. N. R. — Oxidation of methanol on the surfaces of model Cu/AnO catalysts containing Cu^{1+} and Cu^0 species, *Catal. Lett.*, 1997, **47**, 265.

5. HARIKUMAR, K. R., VINOD, C. P. KULKARNI, G. U. AND RAO, C. N. R. — Facile C-O bond scission on Zn surfaces, *J. Phys. Chem. B*,1999, **103**, 2445.

6. HARIKUMAR, K. R. AND RAO, C. N. R. — Role of oxygen transients in the facile scission of C-O bonds on Zn surfaces, *Chem. Commun.*, 1999, 341.

7. HARIKUMAR, K. R., GHOSH, S. AND RAO, C. N. R. — X-ray photoelectron spectroscopic investigations of Cu-Ni, Au-Ag, Ni-Pd and Cu-Pd bimetallic clusters, *J. Phys. Chem. A*, 1997, **101**, 536.

8. HARIKUMAR, K. R., VINOD, C. P. KULKARNI, G. U. AND RAO, C. N. R. — Interaction of CO with Cu-Pd and Cu-Ni bimetallic clusters, *Topics in Catalysis* (Accepted for publication).